Supporting Information

6-Aminocoumarin derived Schiff base gelators: Aggregation and sensing of CN^-, Fe^{3+}, Cu^{2+} and CO_2 under different conditions

Eshani Paul, Rameez Raza, Subrata Ranjan Dhara, Nabajyoti Baildya and Kumaresh Ghosh*

Department of Chemistry,University of Kalyani, Kalyani-741235, India.
Email: ghosh_k2003@yahoo.co.in; kumareshchem18@klyuniv.ac.in

TableS1. Results of gelation test for compounds **1** and compound **2**.

Solvents	Compound 1	Compound 2
$CHCl_3$	S	PS
MeOH	I	I
THF	S	PS
DMF	S	S
DMSO	S	S
CH_3CN	S	S
1,4-Dioxane	S	S
Toluene	I	PS
DMF-H_2O (2:1,v/v)	**G (5 mg/mL)** (T_g = 75 °C)	**G (6 mg/mL)**(T_g = 78 °C)
DMSO-H_2O (2:1,v/v)	**G (4 mg/mL)** (T_g = >80 °C)	**G (5 mg/mL)**(T_g = >80 °C)
Dioxane-H_2O (2:1,v/v)	**G (5 mg/mL)** (T_g = 68 °C)	**G (6 mg/mL)** (T_g = 70 °C)
S = Soluble; G = Gel (minimum gelation concentration); PS= Partially soluble; I= Insoluble.		

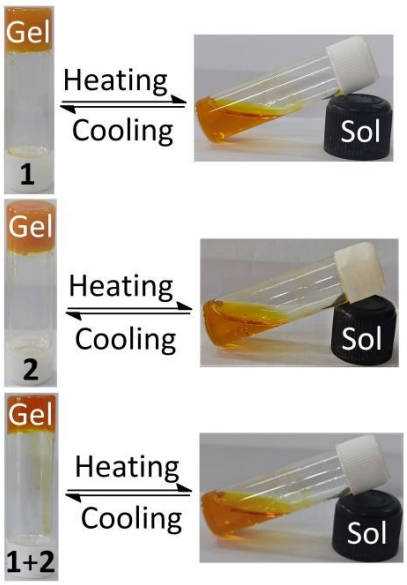

Figure S1.Thermo-reversibility of gel **1** (c =1.35 x 10^{-2} M), gel **2** (c=1.2 x1 0^{-2}M) and mixed gel of **1** and **2** in DMF-H_2O (2: 1, v/v).

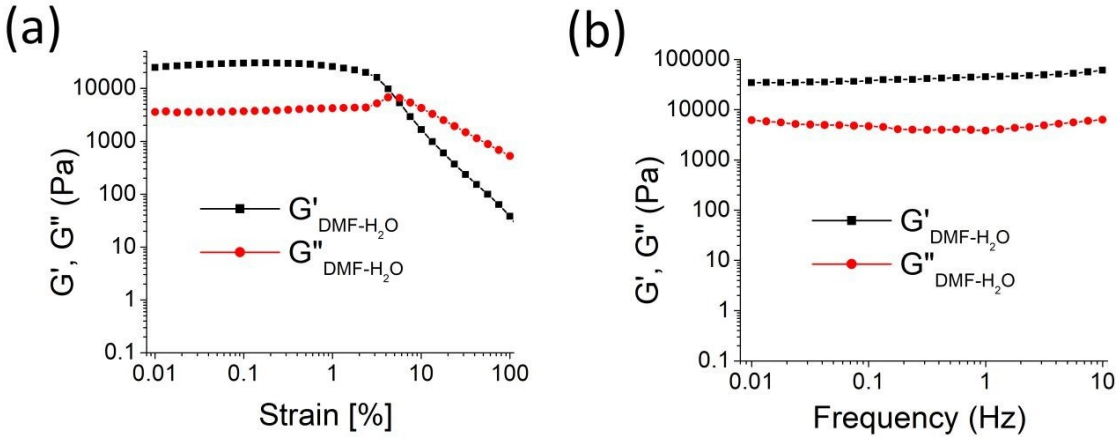

Figure S2. Rheology study of the mixed gel of **1** and **2** in DMF-H_2O (2: 1, v/v): (a) amplitude sweep (at constantfrequency of 1 Hz) and (b) frequency sweep (at constant 0.01% strain) experiments.

Table S2. Summary of rheological properties of mixed gel of **1** and **2.**

Gel in Solvent	Critical strain (%)	Crossover (% strain)	G'_{av}(Pa)*	G''_{av}(Pa)*	G''_{av}/G'_{av}
Mixed gel in DMF-H_2O	1.01	5.10	41852	6212.8	0.148
*G'_{av} a ndG$''_{av}$values were calculated from frequency sweep data.					

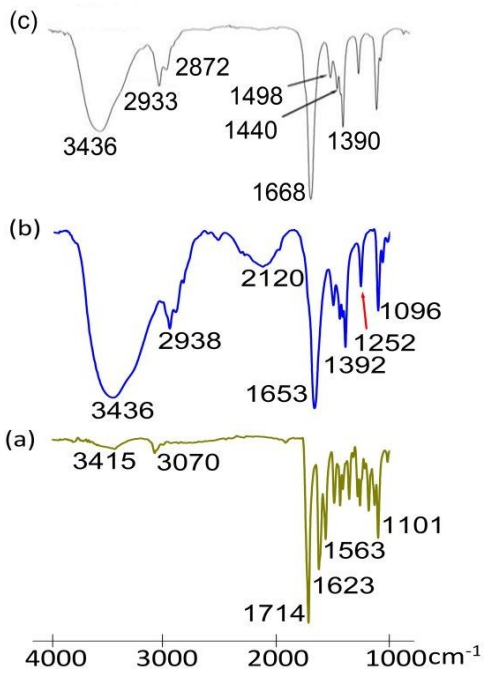

Figure S3. Comparison of FT-IR spectra of **1** in the (a) powder and (b) gel state in DMF-H_2O (2:1, v/v). In the series (c) indicates the FT-IR of DMF solvent.

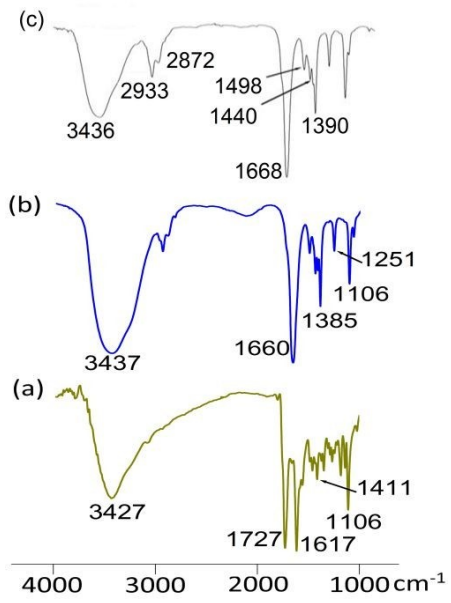

Figure S4. Comparison of FT-IR spectra of **2** in the (a) powder and (b) gel state in DMF-H_2O (2:1, v/v). In the series (c) indicates the FT-IR of DMF solvent.

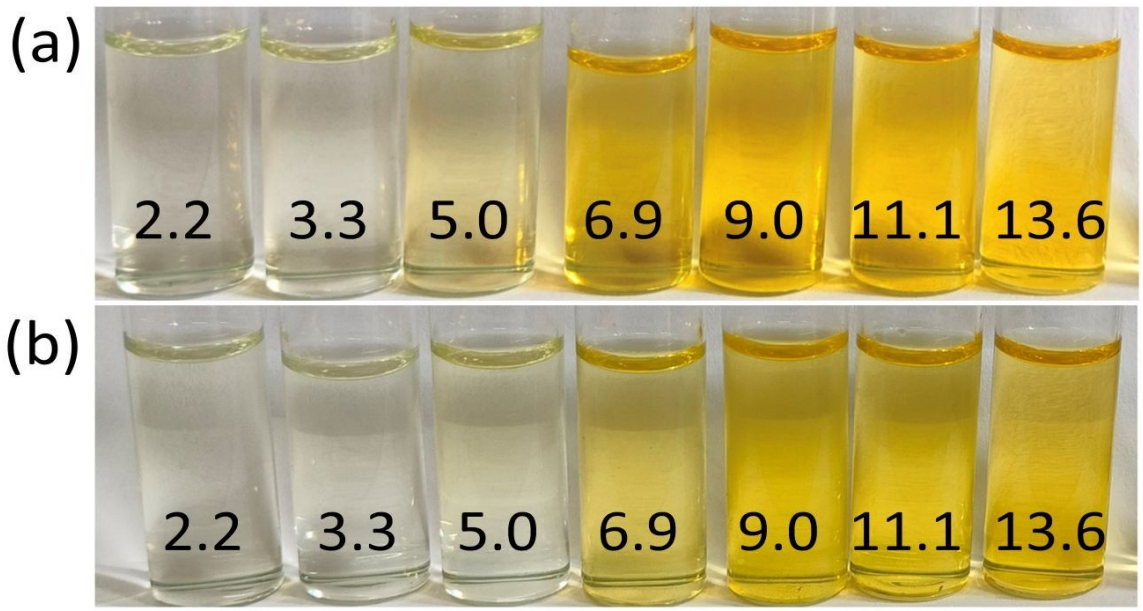

Figure S5. Change in color of solutions of **1** (a) and **2** (b) at different pH values in DMF: H_2O (2:1, v/v).

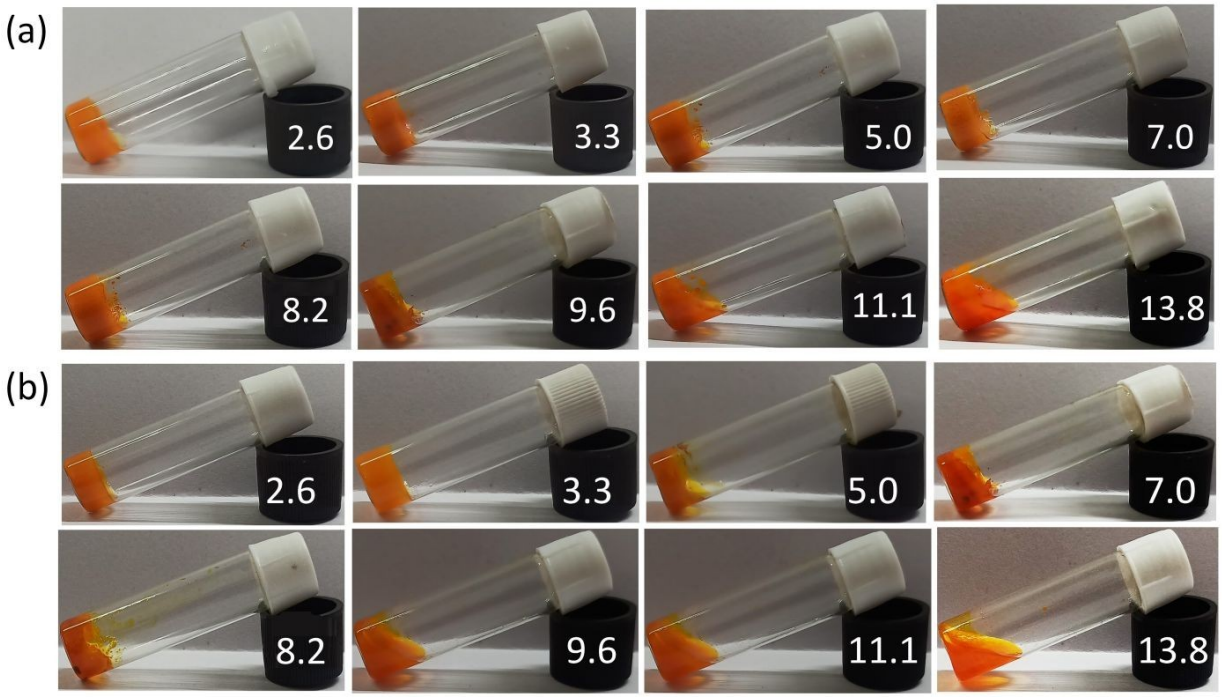

Figure S6. pH variation in DMF-H_2O (2: 1, v/v) gels of **1**(a) and **2** (b).

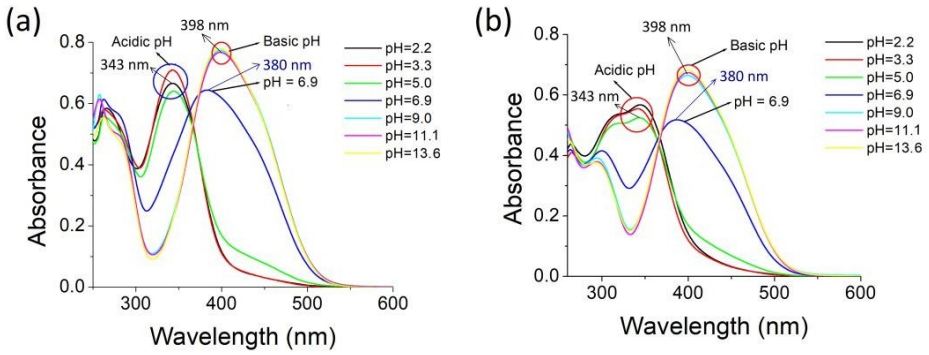

Figure S7. Change in absorbances of **1** (a) and **2** (b) (c = 2.50 x 10^{-5} M) in DMF-H_2O (2:1,v/v) at different pH values.

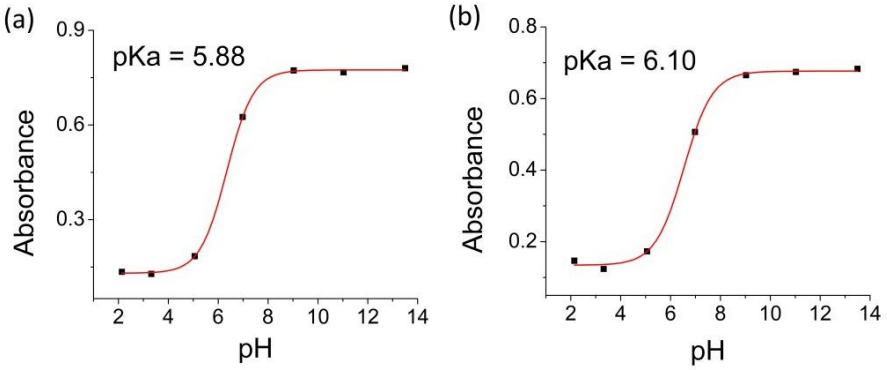

Figure S8. Change in absorbances of **1** and **2** at 380 nm 385 nm, respectively in response to pH change in DMF: H_2O (2: 1, v/v) to determine pKa values.

A.

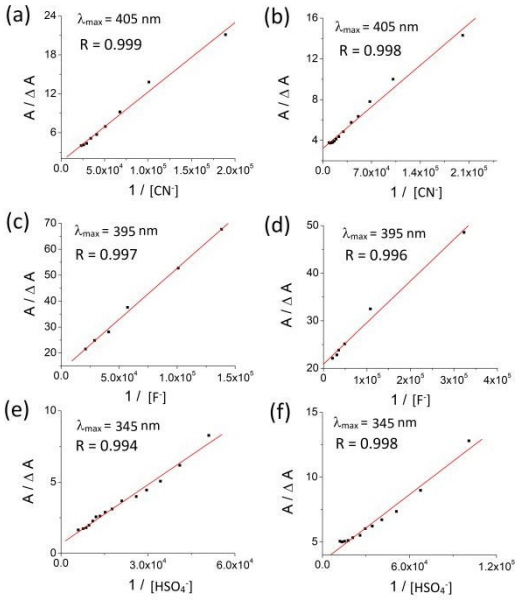

B.

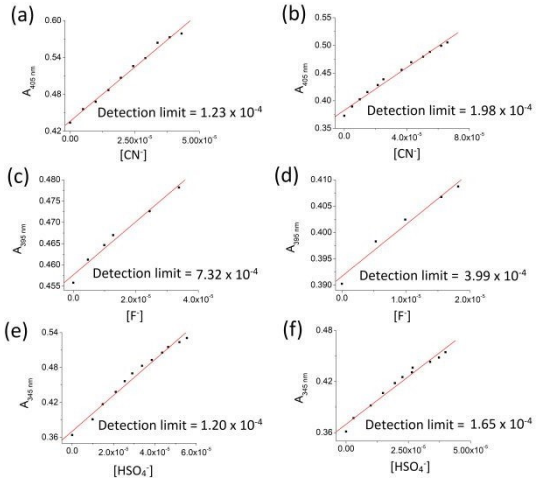

Figure S9. Benesi-Hildebrand plots of A. compound **1** (a, c, e) and compound **2** (b, d, f) using UV-vis titration data; B. Detection limits for the anions (CN^-, F^- and HSO_4^-; c = 1.0 x 10^{-3} M) with **1** (a, c and e) and **2** (b, d and f) (c = 2.5.0 x 10^{-5} M) from UV-vis in DMF-H_2O (2: 1, v/v).

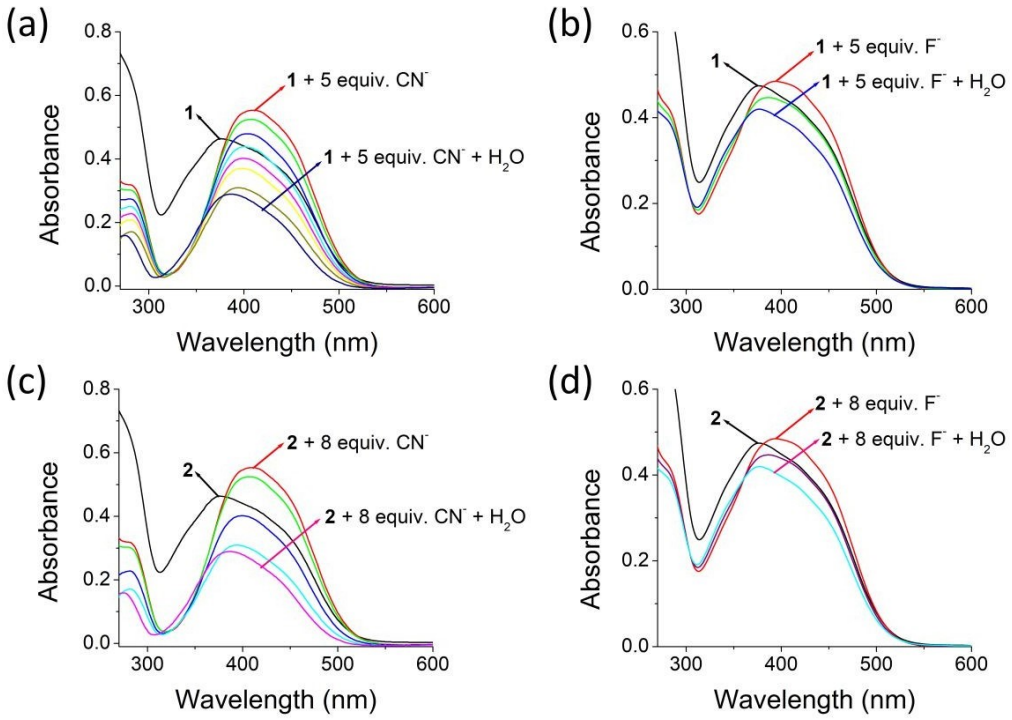

Figure S10. Change in absorbance of (a) **1**.CN^-ensemble (b) **1.**F^- ensemble and (c) **2**.CN^-ensemble (d) **2.** F^-ensemble [prepared from addition of 5 equiv. amounts of CN^- and F^- (c = 1.0 x 10^{-3} M) to **1** (c = 2.50 x 10^{-5} M) and 8 equiv. amounts of $CN^-$and F^- (c = 1.0 x 10^{-3} M) to **2** (c = 2.50 x 10^{-5} M), respectively in DMF-H_2O (2: 1, v/v)] upon addition of H_2O.

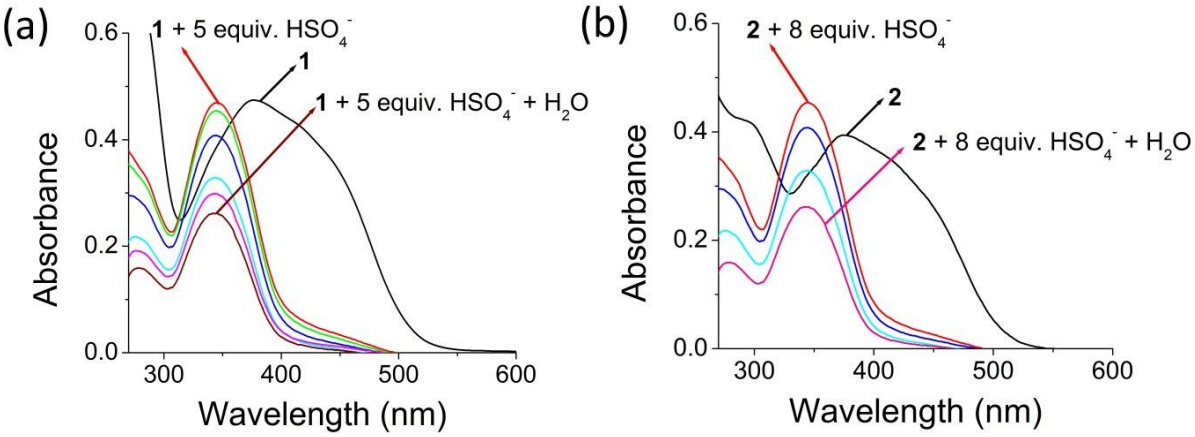

Figure S11. Change in absorbances of the ensembles of HSO_4^- with **1** and **2** [prepared from addition of 5 equiv. amounts of HSO_4^- (c = 1.0 x 10^{-3} M) to **1** (c = 2.50 x 10^{-5} M) and 8 equiv. amounts of HSO_4^- (c = 1.0 x 10^{-3} M) to **2** (c = 2.50 x 10^{-5} M) in DMF-H_2O (2: 1, v/v)] upon addition of H_2O.

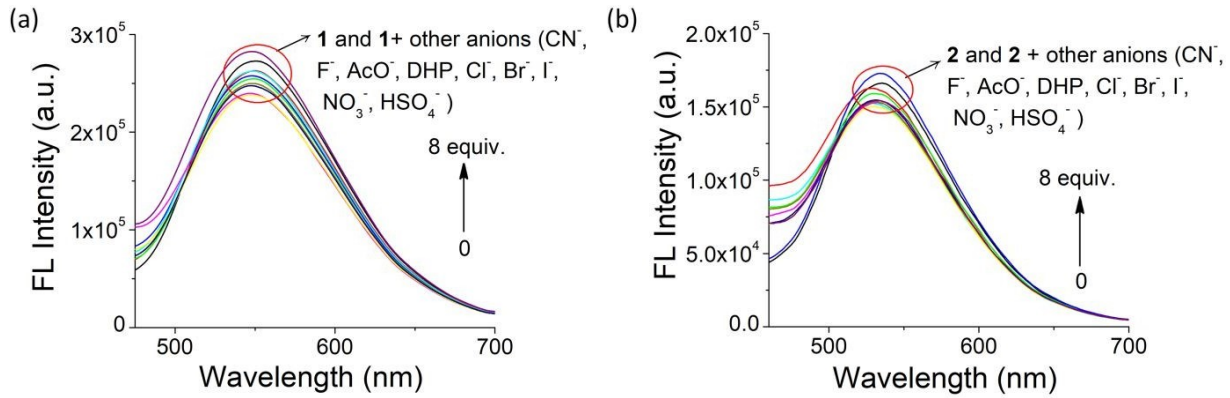

Figure S12. Change in emissions (λ_{exc}= 380 nm) of **1** (a) and **2** (b) (c = 2.50 x 10^{-5} M) in DMF-H_2O (2:1,v/v) upon addition of tetrabutylammonium salts of other anions.

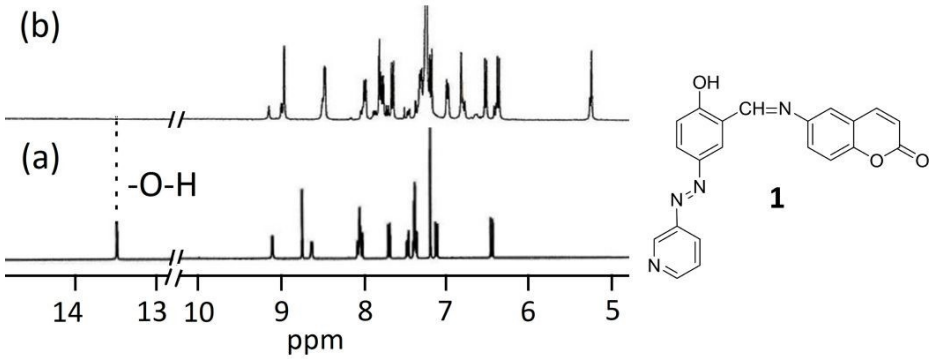

Figure S13. Partial ^{1}H NMR (400 MHz) of **1** (c = 1.08 x 10^{-2} M) in the absence (a) and presence (b) of 1 equiv. amount of CN^- (c = 0.223 M) in $CDCl_3$.

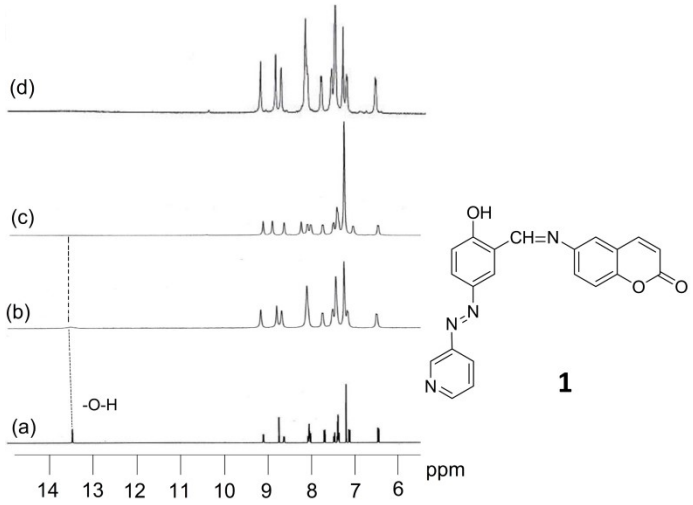

Figure S14. Partial ^{1}H NMR (400 MHz) of **1** (c = 1.08 x 10^{-2} M) in the absence (a) and presence (b) of 0.20 equiv., (c) 0.50 equiv. and (d) 1 equiv. amount of F^- (c = 0.380 M) in $CDCl_3$.

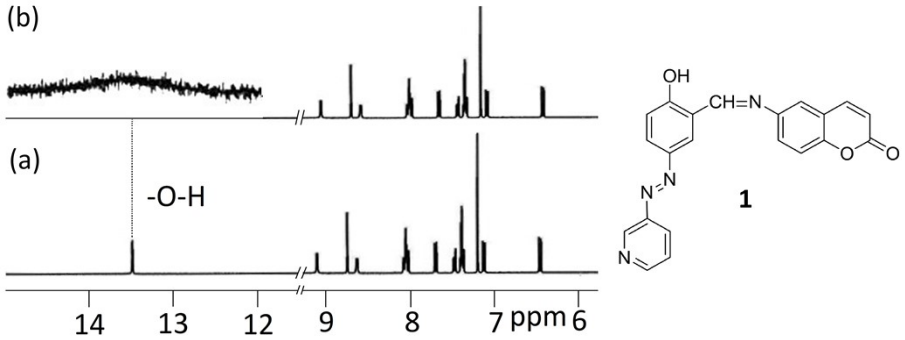

Figure S15. Partial ^{1}H NMR (400 MHz) of **1** (c = 1.08 x 10^{-2} M) (a) in the absence and (b) presence of 1equiv. amount of HSO_4^- (c = 0.353 M) in $CDCl_3$.

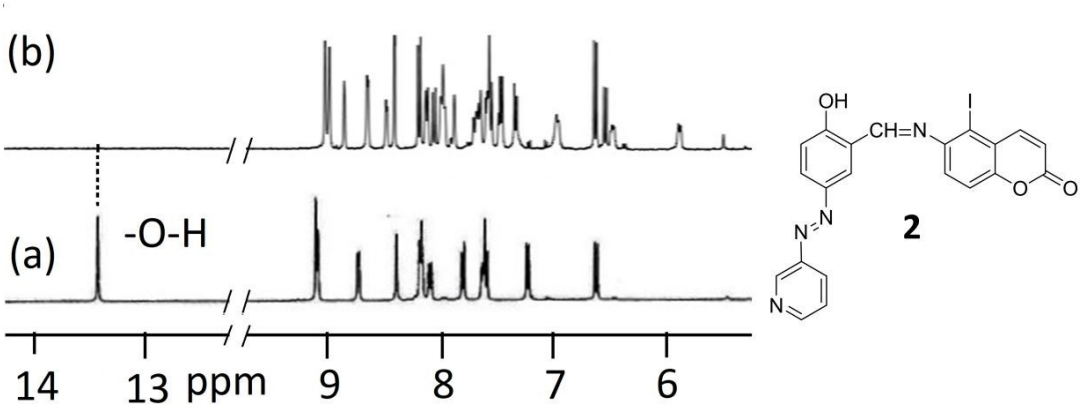

Figure S16. Partial ^{1}H NMR (400 MHz) of **2** (c = 6.0 x10^{-3} M) in the absence (a) and presence (b) of 1equiv. amount of CN^- (c = 0.223 M) in DMSO-d_6.

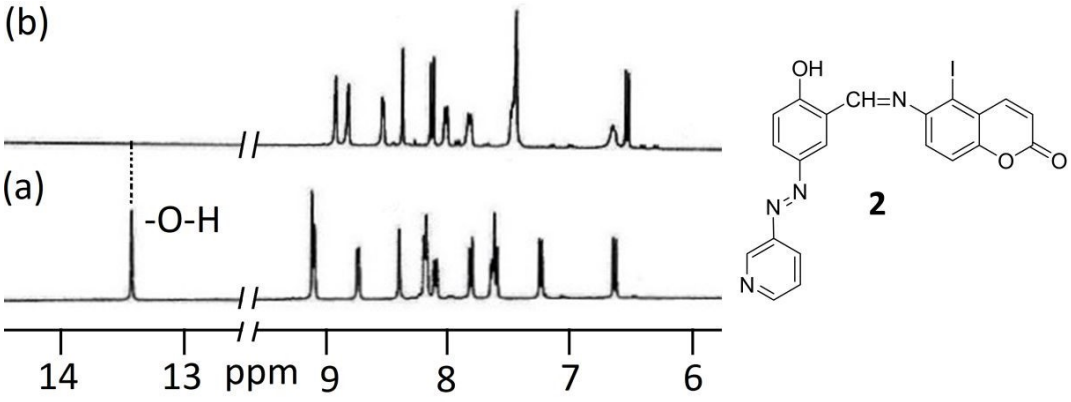

Figure S17. Partial ^{1}H NMR (400 MHz) of **2** (c = 6.0 x 10^{-3} M) in the absence (a) and presence (b) of 1 equiv. amount of F^- (c = 0.380 M) in DMSO-d_6.

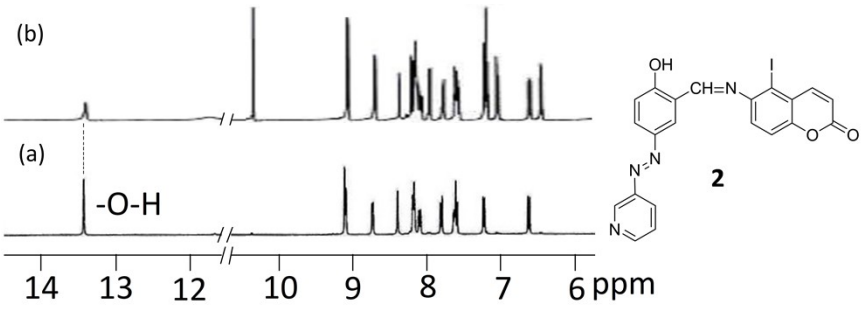

Figure S18. Partial ^{1}H NMR (400 MHz) of **2** (c = 6.0 x 10^{-3} M) in the absence (a) and presence (b) of 1equiv. amount of HSO_4^- (c = 0.353 M) in DMSO-d_6.

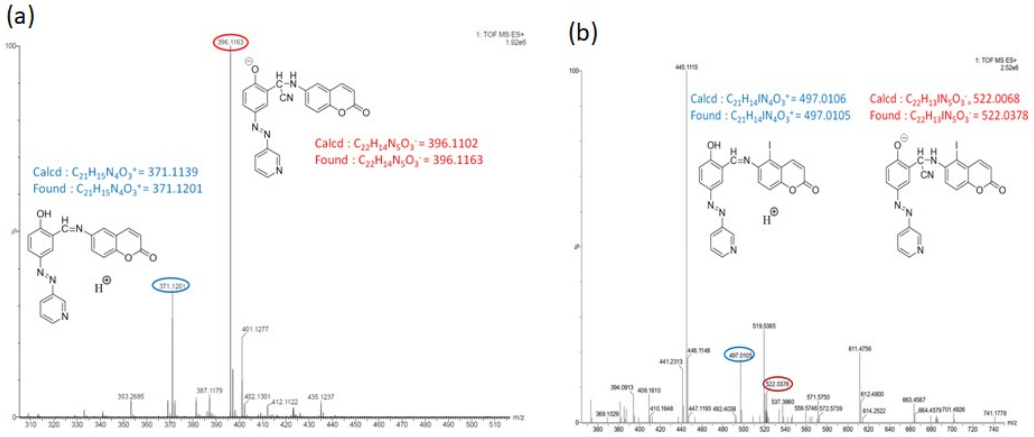

Figure S19. Mass spectra of the cyanide adducts of (a) **1** and (b) **2**.

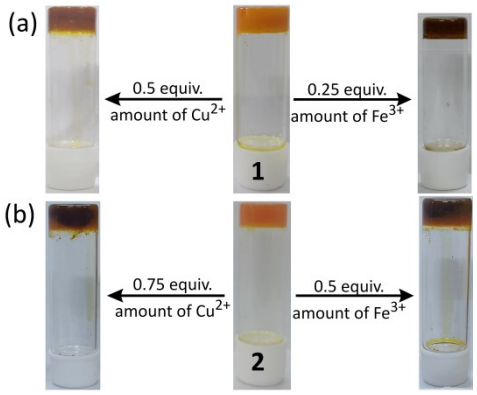

Figure S20. Gel-to-gel color change for DMF-H_2O (2: 1, v/v) gels of **1** (5 mg/mL) and **2** (6 mg/mL) upon addition of minimum amount of $Cu(ClO_4)_2$ and $Fe(ClO_4)_3$.

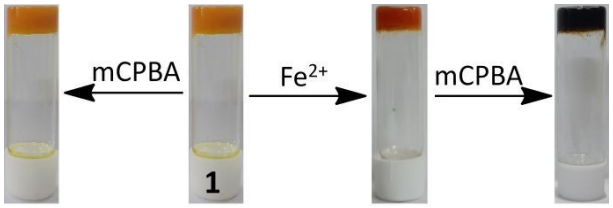

Figure S21. Treatment of *m*-CPBA in Fe^{2+}- induced gel of **1** in DMF-H_2O (2:1,v/v).

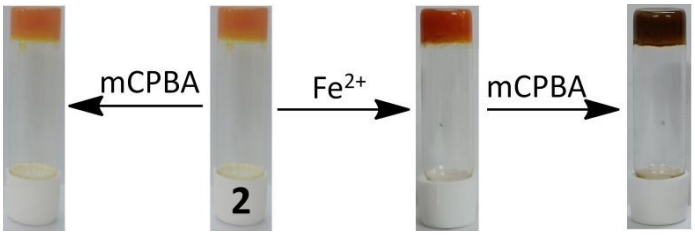

Figure S22. Treatment of *m*-CPBA in Fe^{2+}- induced gel of **2** in DMF-H_2O (2:1, v/v).

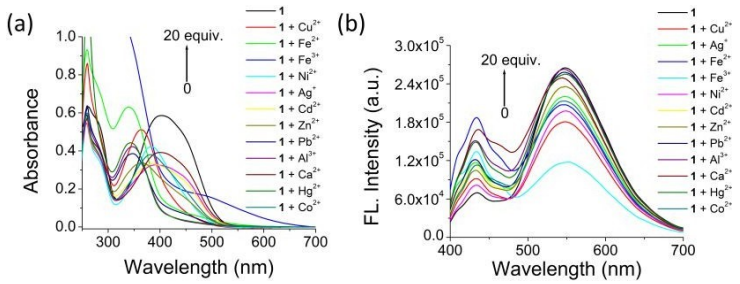

Figure S23. Change in absorbance (a) and emission (λ_{exc} = 380 nm) (b) of **1** (c = 2.5 x 10^{-5}M) upon addition of 20 equiv. amounts of different metal ions (c = 1 x 10^{-3} M) in DMF-H_2O (2:1, v/v).

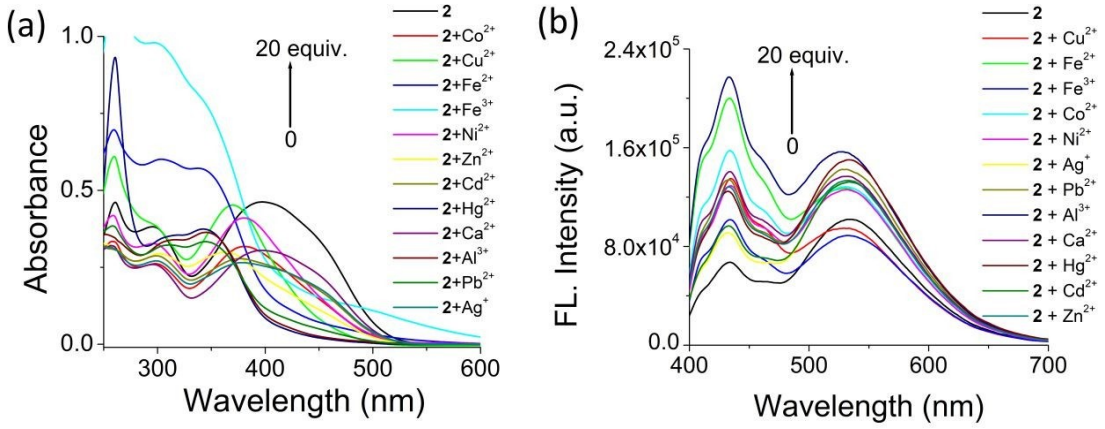

Figure S24. Change in absorbance (a) and emission (λ_{exc} = 380 nm) (b) of **2** (c = 2.5 x 10^{-5}M) upon addition of 20 equiv. amounts of different metal ions (c = 1 x 10^{-3} M) in DMF-H_2O (2:1, v/v).

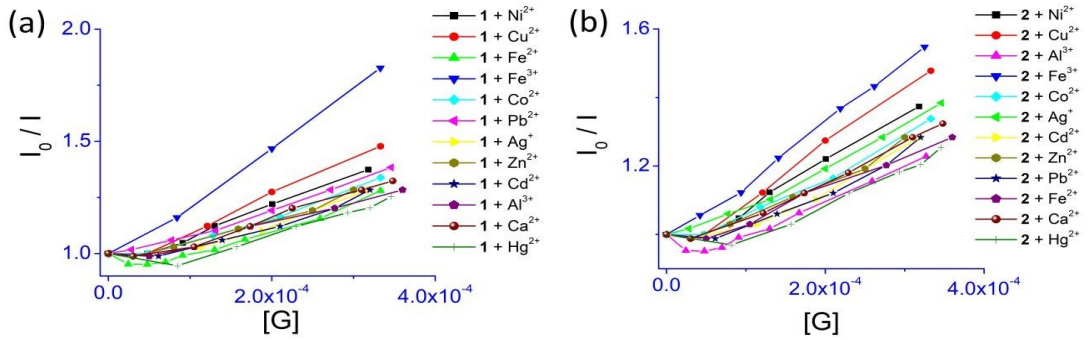

Figure S25. Stern-Volmer plots for compounds (a) **1** and (b) **2** with the different metal ions.

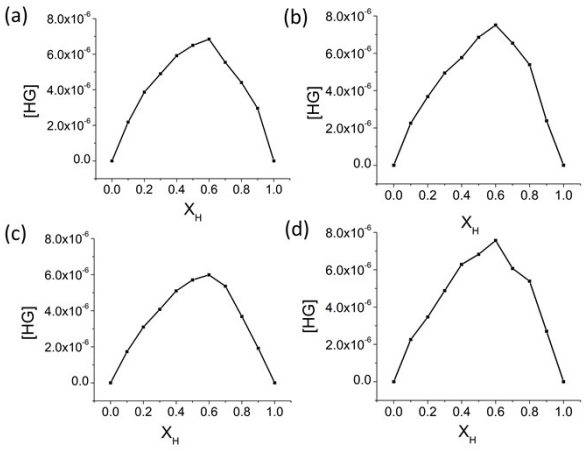

Figure S26. UV-vis Job plots for compound **1** with (a) Cu^{2+} and (b) Fe^{3+} ([H] = [G] = M) compound **2** with (a) Cu^{2+} and (b) Fe^{3+} in DMF-H_2O (2:1, v/v) where [H] = [G] = 2.5 x 10^{-5} M.

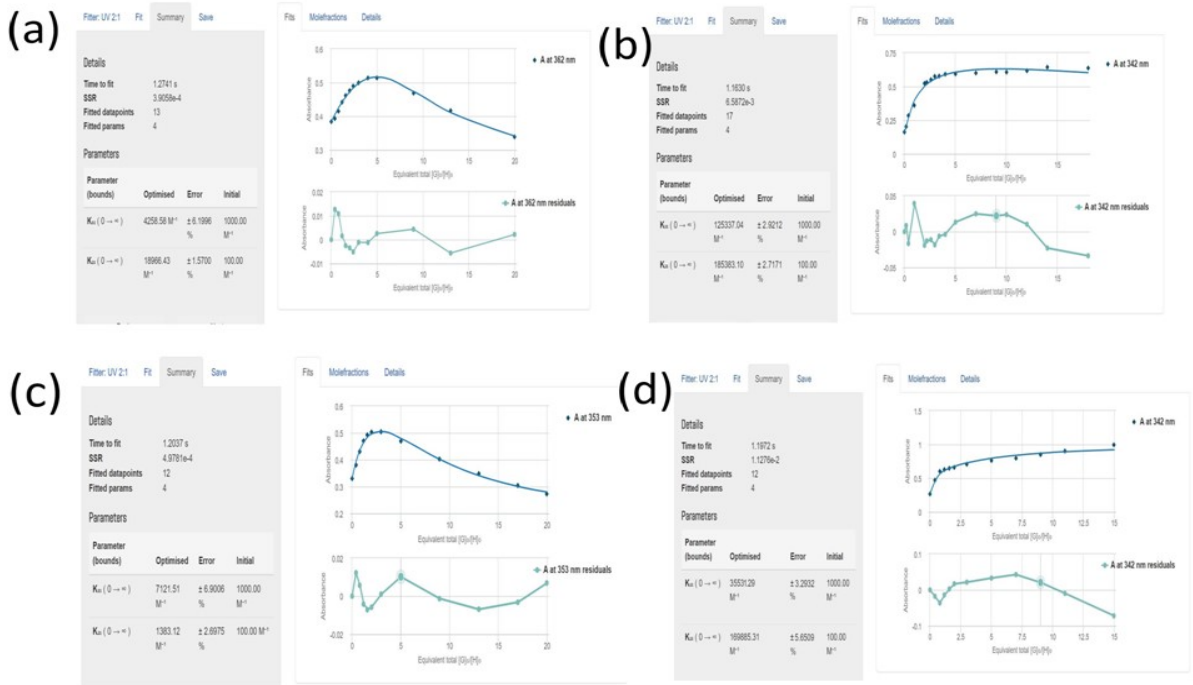

Figure S27. Non-linear fitting of UV-vis titration data for binding constant determination: (a) **1** with Cu^{2+} ions, (b) **1** with Fe^{3+} ions, (c) **2** with Cu^{2+} ions, (d) **2** with Fe^{3+} ions.

Table S3.Crystallographic data and structure refinement of Cu^{2+}-complex of **2**.

Empirical formula	$C_{42}H_{24}CuI_2N_8O_6$
Formula weight	1054.03 g/mol
Temperature/K	298(2) K
Crystal system	triclinic
Space group	P-1
a/Å	8.4881(17)
b/Å	9.0750(18)
c/Å	14.960(3)
α/°	93.295(6)
β/°	105.306(6)
γ/°	92.251(6)
Volume/$Å^3$	1107.9(4)
Z	1
$\rho_{calc}g/cm^3$	1.580
μ/mm^{-1}	1.940
F(000)	515
Crystal size/mm^3	0.056 × 0.089 × 0.152
Radiation	MoKα (λ = 0.71073)
2Θrange for data collection/°	4.50° to 50.50°
Index ranges	-10≤h ≤10, -10 ≤k ≤10, -17 ≤l ≤17
Reflections collected	20628
Independent reflections	3938 [R(int) = 0.1270]
Data/ restraints/ parameters	3938 / 0 / 268
Goodness-of-fit on F^2	1.062
Final R indexes [I > = 2σ(I)]	R1 = 0.1089, wR2 = 0.1656
Final R indexes [all data]	R1 = 0.1975, wR2 = 0.1986
Largest diff. peak/hole /e $Å^{-3}$	1.374/ -0.671
CCDC Number	2361386

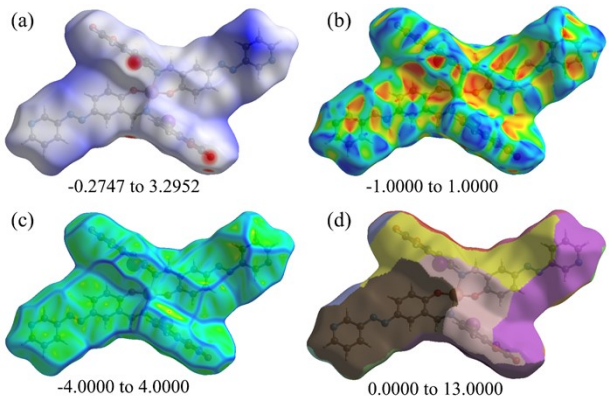

Figure S28. Hirshfeld surfaces of the complex (a) d_{norm}, (b) shape index, (c) curvedness, and (d) fragment patch.

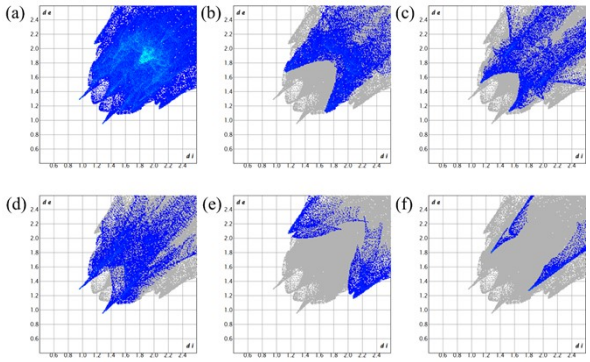

Figure S29. 2D fingerprint plots of the complex (a) all interactions, (b) C···H/H···C interactions, (c) N···H/H···N interactions, (d) O···H/H···O interactions, (e) I···H/H···I interactions, and (f) I···O/O···I interactions.

^{1}H NMR ($CDCl_3$, 400 MHz) of 1

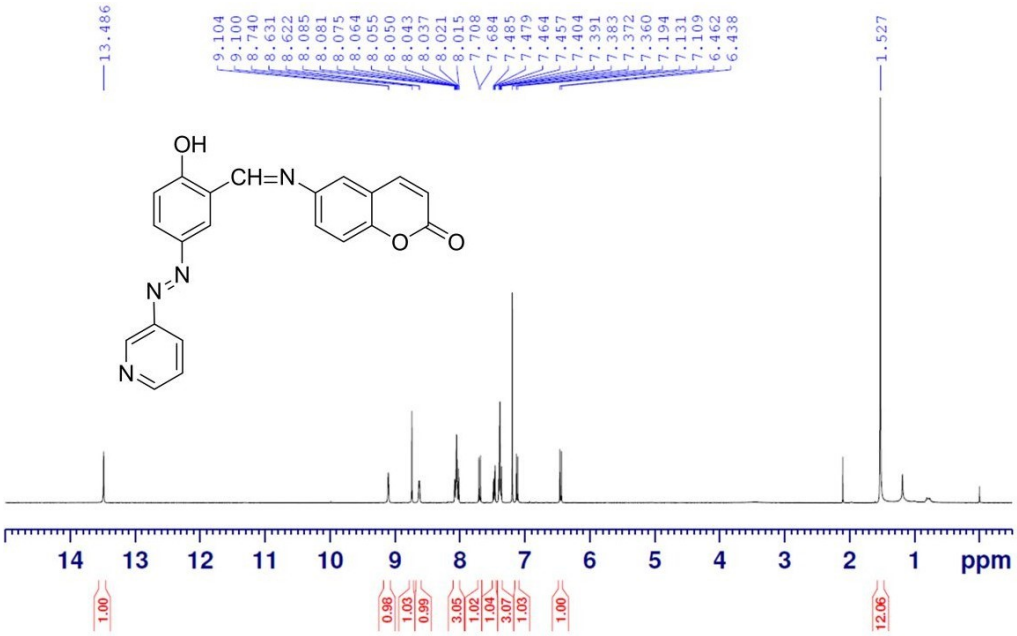

^{13}C NMR ($CDCl_3$, 100 MHz) of 1

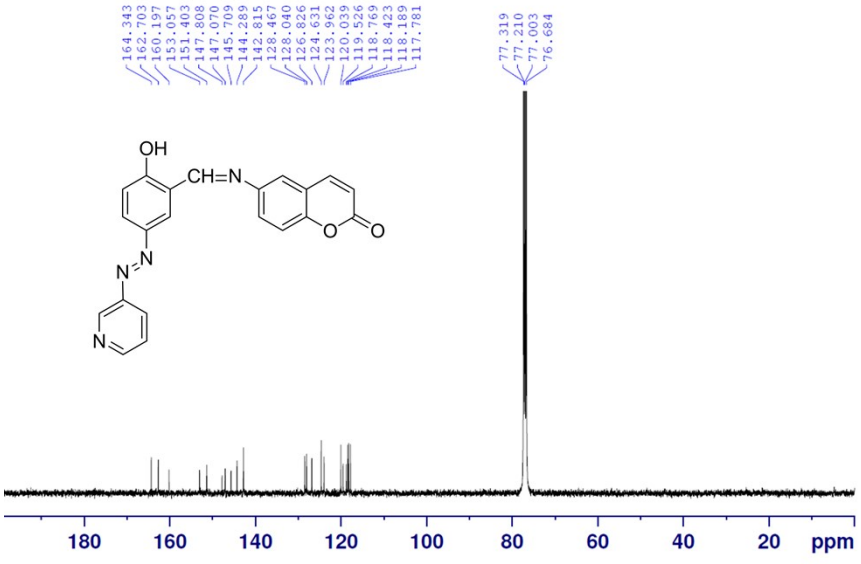

^{1}H NMR (DMSO-d_6, 400 MHz) of 2

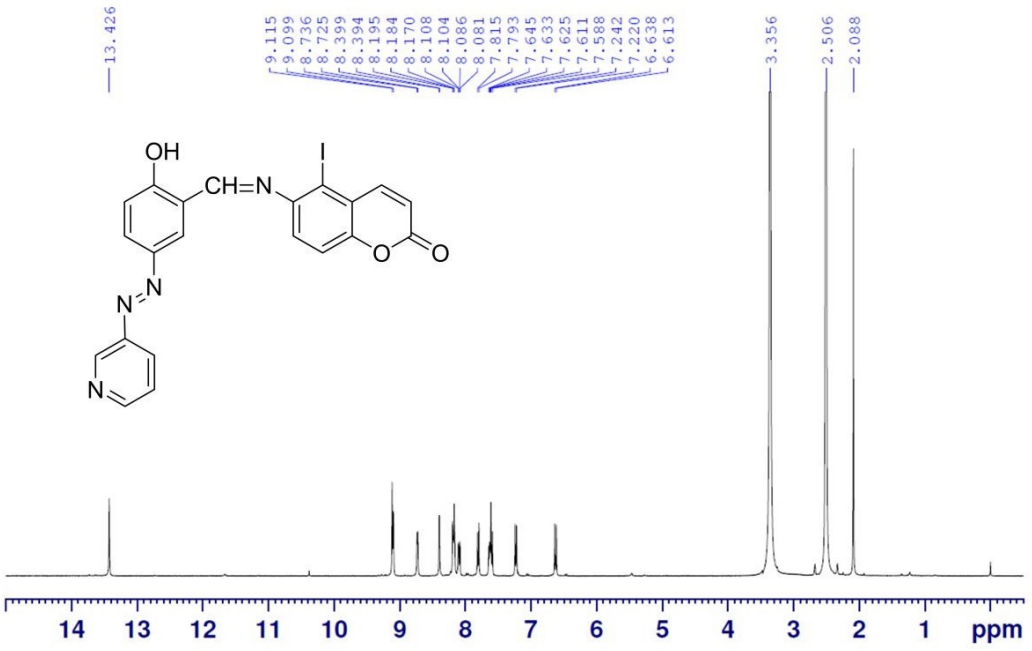

^{13}C NMR (DMSO-d_6, 100 MHz) of 2

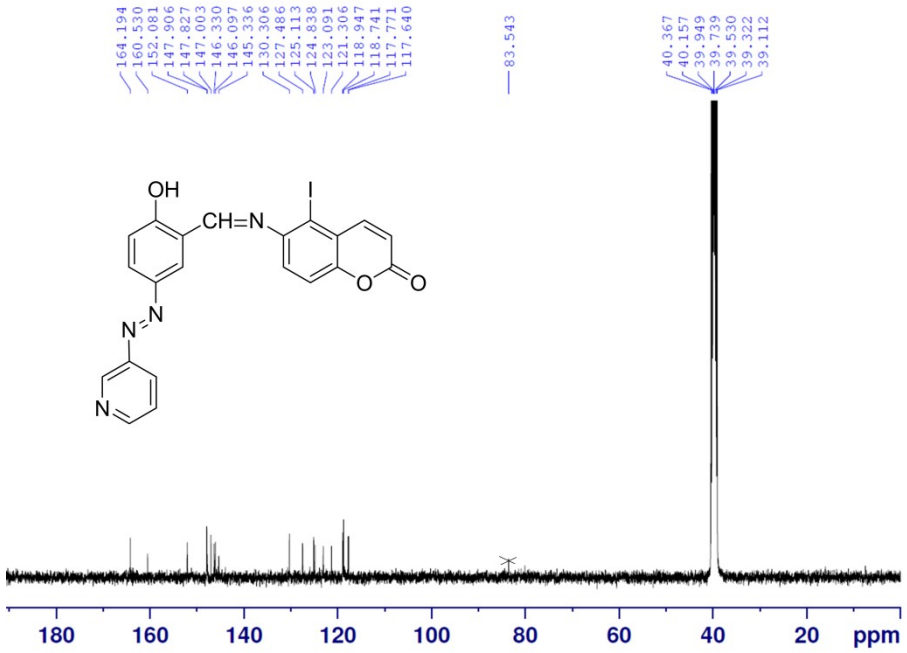

Mass spectrum of 1

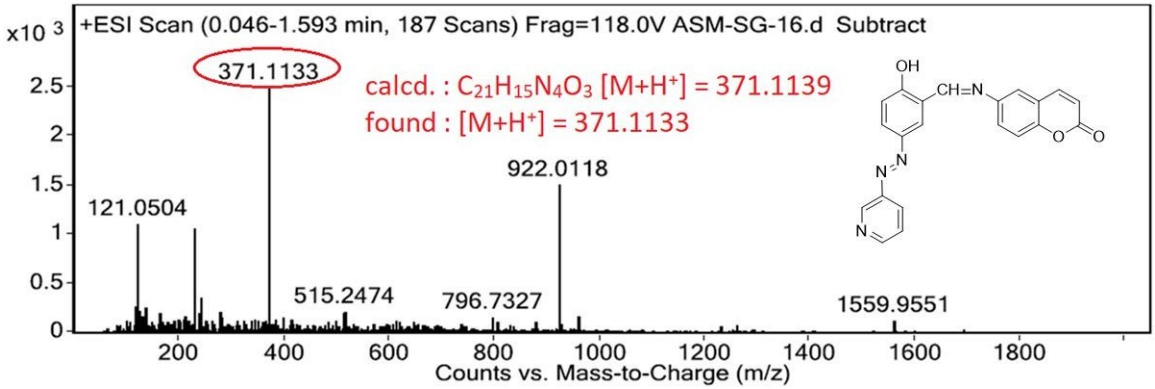

Mass spectrum of 2